RSC Advances

ROYAL SOCIETY OF CHEMISTRY

www.rsc.org/advances

The density functional theory calculation of the oxidative stability and reduction decomposition mechanism is quite an important factor for practical application.

Journal Name

RSCPublishing

ARTICLE

Oxidative stability and reduction decomposition mechanism study on a novel salt: lithium difluoro(sulfato)borate

Shiyou Li, Xiaopeng Li, Hongming Zhang, Liping Mao and Xiaoling Cui[a,*]

Cite this: DOI: 10.1039/xOxxOOOOOx

Received OOth January 2012,
Accepted OOth January 2012

DOI: 10.1039/xOxxOOOOOx

www.rsc.org/

Lithium difluoro(sulfato)borate ($LiBF_2SO_4$) is a novel salt designed for battery electrolyte usage. Limited information is currently available, however, regarding its structure and chemical characteristics. The density functional theory calculation has therefore been used to explore both of the oxidative stability and the reduction decomposition mechanism of $LiBF_2SO_4$. The results show that oxidation potential (E_{OX}) for $LiBF_2SO_4$ could be calculated by using the correlation between the highest occupied molecular orbital energy and the corresponding E_{OX}. Besides, reduction decomposition mechanism of $LiBF_2SO_4$, especially at high potential about 1.7 V (vs Li/Li^+) during the first discharge, is calculated. In addition, many other electrolyte salts have also been investigated, to broaden the current knowledge of the use of chelato-borates as electrolyte components, to design and select high-performance electrolyte salts for lithium ion batteries, and to predict the chemical and physical characteristics of screening electrolyte salts, with the intent of using this induction for up-coming projected missions.

Introduction

Since the highest gravimetric and volumetric energy densities, lithium ion batteries (LIBs) have become one of the most important commercially produced rechargeable batteries [1]. Coupled with developments of electric vehicles and hybrid electric vehicles, there is increased demand for LIBs with better performance for higher power capability, rate capability and wide-temperature cycle performance [2]. Electrolyte has a significant impact upon the battery. And a solution of lithium hexafluorophosphate ($LiPF_6$) in a mixture of carbonate solvents is most widely used as a commercial nonaqueous electrolyte in today's state-of-the-art LIBs [3]. However, the preferred salt, $LiPF_6$, has given rise to certain drawbacks, for its limited thermal stability and high sensitivity to trace moisture in the air [4]. To address this issue, numerous efforts have been attempted to the development of alternative salts for electrolytes of LIBs.

One interesting class of substances, which has been proposed both as electrolyte salt and electrolyte additive, is lithium chelato-borate salts [5]. Very recently, our group has reported a novel salt named lithium difluoro(sulfato)borate ($LiBF_2SO_4$), which shows many better electrochemical properties than LiPF6, such as excellent facilitation for the formation of effective and conductive solid electrolyte interphase (SEI) films on the electrodes (especially carbon), and for the improvement of cells' life characteristics [6].

With the intent of finding optimized electrolyte salts for LIBs, during the last decades, computational chemistry methods have become powerful tools to investigate molecular properties even if they are hardly accessible in experiments. Besides, computational chemistry methods can predict characteristics and behavior of molecules without the need for actually synthesizing them [5]. Considering its accuracy and reliability, the density functional theory (DFT) calculation is recommended as a useful tool for screening electrolyte salt for LIBs [7]. Using a high-accuracy DFT calculation, the structures of intermediate radicals and novel salt molecules are determined.

For this reason, the primary focus of our work has been to understand and predict the structure and chemical characteristics of the novel salt as $LiBF_2SO_4$. In addition, many other electrolyte salts

have also been investigated, such as lithium bis(oxalato)borate (LiBOB), lithium difluoro(oxalato)borate (LiODFB), lithium bis[1,2-benzenediolato(2-)-O,O']borate (LBBB), lithium (malonatooxalato)borate (LiMOB), lithium tetrafluoroborate ($LiBF_4$), $LiPF_6$, and lithium perchlorate ($LiClO_4$). Anion structures of theses electrolyte salts are shown in Fig. 1. The worthwhile aim is to broaden the current knowledge of the use of chelato-borates as electrolyte components, to design and select high-performance electrolyte salts for LIBs, and to predict the chemical and physical characteristics of screening electrolyte salts, with the intent of using this induction for up-coming projected missions.

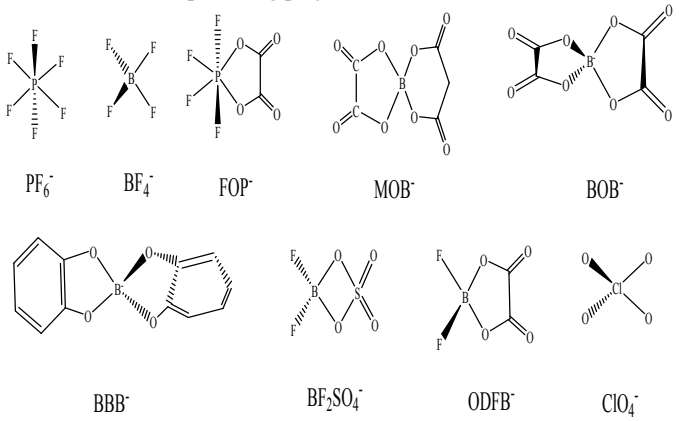

Fig. 1. Anion structures of typical electrolyte salts. Computational details

Computational details

The calculations were performed using the Gaussian 09 program package [8]. The structures of involved reactants and products were optimized by B3LYP/6-311++G(d, p) method [9,10]. To confirm each optimized stationary point, frequency analyses were done with the same basis set. Energy and Gibbs free energy were obtained at 298.15 K. Vibration frequency and intrinsic reaction coordinate (IRC) analyses were employed to confirm all the transition states of the reaction pathways at the same level.

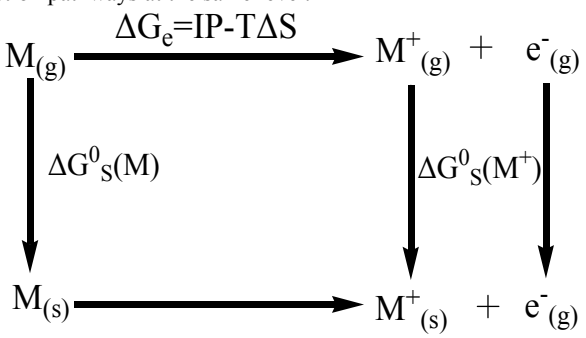

Fig. 2. Free-energy cycle for the redox reaction ($M \rightarrow M^+ + e^-$), where $M_{(g)}$ denotes molecule M in the gas-phase, $M_{(S)}$ denotes the solvated molecule, and IP denotes ionization potential.

The oxidation potential E_{OX} could be calculated from the energy cycle shown in Fig. 2. It was converted from the absolute E_{OX} to the potential vs. Li^+/Li by a factor of 1.4 V, as shown in Eq. (1) [11],

$$E_{ox}(Li/Li^+) = \frac{IP + T\Delta S(M) - T\Delta S(M^+) + \Delta G_s^0(M^+) - \Delta G_s^0(M)}{F} - 1.4\text{V} \quad (1)$$

where ΔG_e is the ionization free energy in the gas-phase at 298.15 K; $\Delta G_S(M^+)$ and $\Delta G_S(M)$ are the free energies of solvation of the oxidized and initial complexes M^+ and M, respectively; and F is the Faraday constant. The ionization free energy ΔG_e has contributions from the ionization potential that include the adiabatic ionization energy and zero point vibrational correction as well as the entropic term $-T\Delta S$.

Note that, the thermal contribution to the free energy difference is expected to be rather low which found absolute values below 0.04 V over ten organic molecules [12]. Furthermore, the calculation of the quantities needed turned out to be technically demanding. Consequently, it will be neglected in the following, and the standard free energy in solution without thermal contribution constitutes the basis of the E_{OX} according to Eq. (1). For details see literatures [12] and [13].

In order to get the free energy in typical solvent, an effect solvent with dielectric properties of 1,2-ethanediol (dielectric constant = 40.2) was utilized via a polarized continuum model (PCM) [14]. The dielectric constant of 40.2 would be expected in a typical mixed linear and cyclic carbonate electrolytes commonly used in LIBs.

Experimental details

LiBOB [15], LiODFB [16] and $LiBF_2SO_4$ [6] with the purity of about 99.5% (by weight) were synthesized in our laboratory as described previously. 1.0 mol L^{-1} $LiPF_6$-ethylene carbonate (EC)/dimethyl carbonate (DMC) (with the volume ratio of 1:1, the same below), anhydrous EC and anhydrous DMC were produced by Zhangjiagang Guotai Huarong New Chemical Materials Co. Ltd. Electrolyte systems were prepared in a glove box by dissolving 0.7 mol L^{-1} LiBOB, 1.0 mol L^{-1} LiODFB and 1.0 mol L^{-1} $LiBF_2SO_4$ in a mixed solvent of EC/DMC, respectively.

Electrochemical windows of the electrolytes were measured in a three electrode system (the negative electrode was used as a working electrode with a reaction area of 1 cm^2, and lithium sheets were used both as the counter electrode and the reference electrode, respectively) for the cyclic voltammetry (CV), through a CHI660C Electrochemical Workstation (Shanghai, China) at the scan rate of 2 mV s^{-1} in the voltage range of 3.0 to 6.0 V.

Results and discussion

The "model" systems of $BF_2SO_4^-$ and $Li^+BF_2SO_4^-$

First, we present and discuss the results about the "model" systems of $BF_2SO_4^-$ and $Li^+BF_2SO_4^-$. Based on previous studies, the total energy order for lithium tetrafluoroborate ion pairs is bidentate < tridentate < monodentate [17]. This is, a common feature exists for the energy of lithium complexes, and the bidentate structure has the lowest total energy calculated for these isolated ion pairs. Thus, only the optimized geometries of the bidentate ion pairs in solvent are given in Fig. 3.

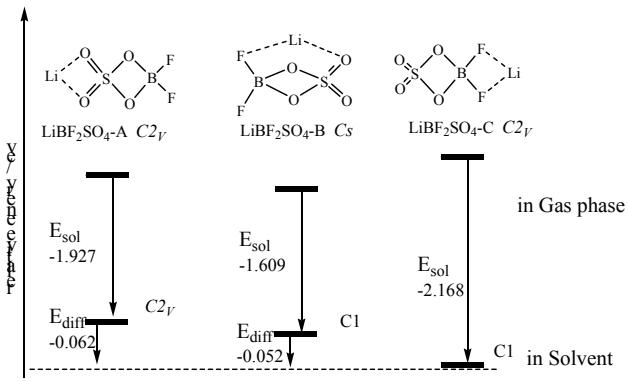

Fig.3. The optimized geometries, symmetries and energies of different $Li^+BF_2SO_4^-$ model structures (A, B, and C). Relative energies (eV) of those models are performed without and with the selected solvent, respectively.

The computational studies consisting of first-principle calculations of the geometries, symmetries and energies for different $Li^+BF_2SO_4^-$ model structures (A, B and C) are shown in Fig. 3. Three different structures would be acquired since Li^+ ions could coordinate with different atoms, labeled as $LiBF_2SO_4$-A, $LiBF_2SO_4$-B and $LiBF_2SO_4$-C, respectively. The total energy of $LiBF_2SO_4$-B is -931.502 Ha, slightly lower than that of the other two structures in gas phase (-931.490 Ha for $LiBF_2SO_4$-A and -931.483 Ha for $LiBF_2SO_4$-C, respectively). It suggests that $LiBF_2SO_4$ may exist in the form of $LiBF_2SO_4$-B in gas phase. But it is amusing that the total energy of $LiBF_2SO_4$-C becomes the minimum (-931.5634 Ha) in the selected solvent, lower than -931.5611 Ha for $LiBF_2SO_4$-A and -931.5615 Ha for $LiBF_2SO_4$-B, respectively. It indicates that $LiBF_2SO_4$-C enjoys the largest stabilization (Esol = -2.168 eV), due to the biggest change of net energy. Salt structure is sensitive to solvent, as noted above, and further studies show that this trend would be enhanced for high dielectric constant solvents. That is to say, $LiBF_2SO_4$-C is favorable to stability in high dielectric constant solvents. That pose a puzzling question that solvent has different effect on $LiBF_2SO_4$ and LiODFB. According to the previous reports, LiODFB has also been identified as three different structures by DFT calculations, similar to $LiBF_2SO_4$ model structures, but LiODFB-A ion pair has been found to be strongly energetically favored for all calculation methods employed [18]. Furthermore, as this type of bidentate $ODFB^-$ coordination via the carbonyl oxygen atoms is found in many of the crystalline solvates, both the computational and experimental results suggest that there is a strong preference for this type of coordination. The reason of this different stable model structures between $LiBF_2SO_4$-C and LiODFB-A ion pairs may due to the fact that the electron density has been conjugated to electron-withdrawing $-SO^{2-}$ groups for $LiBF_2SO_4$ salt.

Table 1. Optimized geometries of the free anion and lithium ion pair[a,b].

a. Bond lengths in Å, bond angles and dihedral angles in degrees.

	$BF_2SO_4^-$	$LiBF_2SO_4$		$BF_2SO_4^-$	$LiBF_2SO_4$
r(B2-O1,3)	1.532	1.517	α(F4-B2-F5)	112.042	110.508
r(B2-F4)	1.378	1.373	α(F4-B2-O1)	112.737	114.038
r(B2-F5)	1.378	1.404	α(O8-S6-O7)	117.059	117.441
r(S6-O1)	1.604	1.608	α(Li9-F5-B2)		130.019
r(S6-O3)	1.604	1.608	d(O7-S6-O3-	112.886	112.636
r(S6-O7)	1.456	1.454	d(F4-B2-F5-	128.447	128.280
r(S6-O8)	1.456	1.454	d(F4-B2-O3-	115.958	118.496
r(F5-Li9)		2.059	d(9Li-F5-B2-		0.00000
r(F4-Li9)		3.223	d(9Li-F5-B2-		128.280

b. Optimized with the DFT method at B3LYP/6-311++G(d,p) level in the selected solvent.

To further study the electroweak interaction between solute and solvent, geometries of $BF_2SO_4^-$ and $LiBF_2SO_4$ were performed. Compared with free $BF_2SO_4^-$, structural changes of the divalent salt are shown in Table 1 and Fig. 4. When $BF_2SO_4^-$ coordinates with Li^+, as expected, (a) the cation-unbounded S6-O1 and S6-O3 distances are lengthened by 0.004 Å, whereas the cation-bounded S6-O7 and S6-O8 distances are shortened by 0.002 Å, respectively; (b) the B2-F4 distance is shortened by 0.005 Å, while the B2-F5 distance is lengthened by 0.026 Å; (c) the Li-F bond length gradually becomes larger than the sum of ionic radii of Li^+ and F atom, suggesting that it has interactions between Li^+ and F atom; (d) the F4-B2-F5 angle decreases by ca. 1.534°, indicating that a distortion occurs when $BF_2SO_4^-$ coordinates with Li^+; (e) except for the two rings keeping in planar surfaces, the geometry of $BF_2SO_4^-$ is distorted for the $LiBF_2SO_4$ ion pair, as shown in Fig. 3, because of the strong interaction between Li^+ and $BF_2SO_4^-$ in the solvent; and (f) consequently, the F4-B2-O3-S6 dihedral angle increases by 2.538°, the O7-S6-O3-O1 dihedral angle decreases by 0.25°.

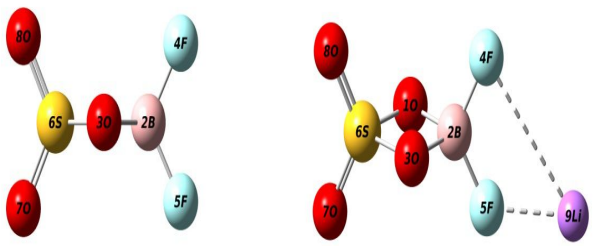

Fig. 4. Optimized geometries of $BF_2SO_4^-$ and $LiBF_2SO_4$. The O, S, B, F and Li atoms are represented, respectively, by red, yellow, pink, dark green and purple spheres. (For interpretation of the references to color in this figure legend, the reader is referred to the web version of this article.)

Prediction of Eox

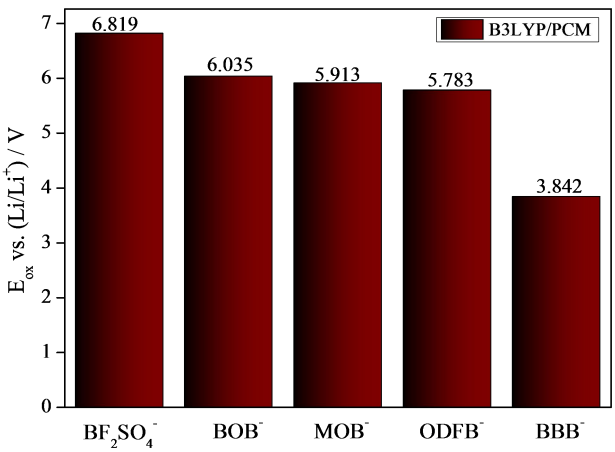

Fig. 5. E_{OXs} of five typical chelate salt anions calculated at the B3LYP/6-311++G(d,p) level for the PCM model.

The experimental electrochemical window for Li-ion battery usually focuses on the onset of the oxidation process, so E_{OXs} of five typical lithium chelato-borate salts were measured against the Li+/Li electrode at B3LYP level of theory for solvation model (PCM). As shown in Fig. 5, the E_{OXs} of those chelato-borate salts can be changed from 3.842 to 6.819 V (vs Li/Li^+) by different chelate effect for the boron atoms. F or BBB^-, $ODFB^-$, MOB^- and BOB^- anions which have been reported earlier, it must be noted that the inaccuracy has been introduced, and the predictive Eoxs are higher than the experimental ones, respectively [5,6,19,20]. It indicates that the PCM model is not perfect enough to predict E_{OX} without any inaccuracy, and should be improved in the future.

But the predictive method can develop models in general, and can range the electrolyte salt in the order of E_{OX}. It suggests that the E_{OX} of $BF_2SO_4^-$ is higher than any of the other typical lithium chelato-borate salts. The reason may be due to the effect of strong electron-withdrawing $-SO_2^-$ groups, which can make good distribution of electron density and give rise to the formation of a stable large π-conjugated system.

To understand the distribution of electron density, in Fig. 6, we plot the mulliken charge analysis of $BF_2SO_4^-$ and $ODFB^-$ radicals, which are typical chelato-borate complexes anions and have the most similar geometry to each other. It can be seen that the electron density of $BF_2SO_4^-$ radical is more distributed than that of $ODFB^-$ radical. Because a good distribution of electron density is good for the energy balance and can mitigate the trend of charge transfer, the E_{OX} of $BF_2SO_4^-$ radical will be higher than that of $ODFB^-$ radical.

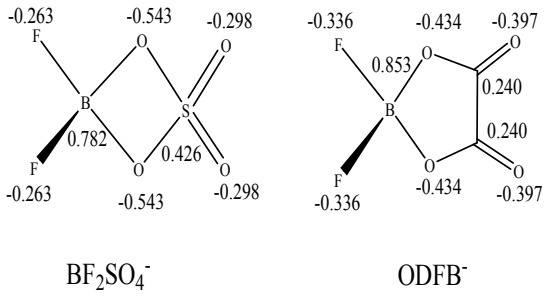

Fig. 6. Mulliken charge on the heavy atoms between $BF_2SO_4^-$ and $ODFB^-$ radicals.

Oxidation decomposition mechanism of $BF_2SO_4^-$-e complex

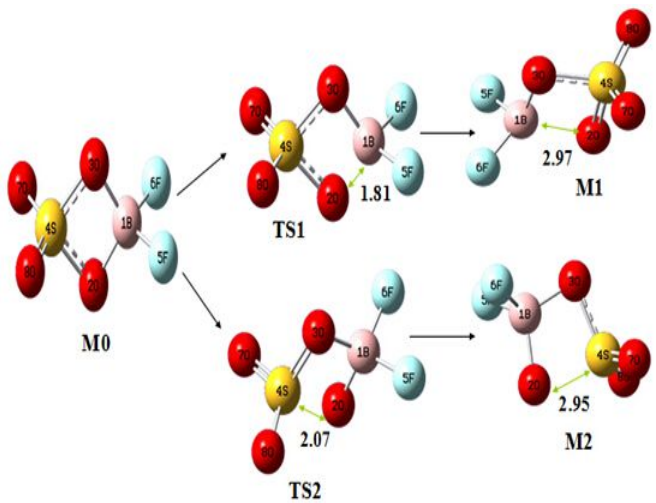

Fig. 7. Optimized structures and bond length (in Å) of the oxidation decomposition products of isolated $BF_2SO_4^-$-e in solvent phase.

The initial oxidation of $BF_2SO_4^-$ involves a one-electron transfer from $BF_2SO_4^-$ anion to cathode, resulting in radical cation ($BF_2SO_4^-$-e). On the basis of the geometry of $BF_2SO_4^-$-e, it can be known that there are two possible pathways for its decomposition, involving two different ring-opening reactions by breaking O−B and S−O bonds, as shown in Fig. 7, respectively. As possible transition states and decomposition products, TS1, TS2, M1 and M2 are also displayed in Fig. 7. All of these TSs have been further confirmed to connect the relative reactant and product by the IRC calculations. Relative energy (in kJ mol^{-1}) and imaginary frequency (ω in cm^{-1}) of the stationary points are listed in Table 2 (the energies are relative to $BF_2SO_4^-$-e). The imaginary frequency shown in Table 2 indicates that the corresponding structures are transition states.

On the basis of the activation energy changes, it can be found that M1 is more stable than M2, and the path with the transition state of TS1 has lower barrier than the path with the transition state of TS2. It suggests that the oxidation decomposition mechanism is much more likely to involve TS1 and M1, and the ring-opening reaction is taken place by broken O−B bond rather than S−O bond. The inference exactly coincides with the ring-opening reaction decomposition for isolated BOB^--e in solvent phase [21]. This result in turn could verify the high E_{OX} of $BF_2SO_4^-$ radical, due to the fact that the relative charge difference between B and O atoms for $BF_2SO_4^-$ radical (0.239) is slightly lower than that for $ODFB^-$ radical (0.419), as shown in Fig. 6.

Table 2. Relative energies (in kJ mol^{-1}) and imaginary frequency (ω in cm^{-1}) of the stationary points of the decomposition reaction of $BF_2SO_4^-$-e complex.

	M0	TS1	M1	TS2	M2
ΔE	0	996.4	900.1	1069.3	946.1
ω	-	-198	-	-438	-

Correlation between the highest occupied molecular orbital energy and the corresponding E_{OX}

Due to the fact that there is unmistakable and obvious inaccuracy for the predictive Eoxs shown in Fig. 5, it is necessary to find a new way to predict E_{OX}. Based on the molecular orbital theory, the ability of one molecule to lose or gain an electron depends on the energy level of the highest occupied molecular orbital (HOMO) or the lowest unoccupied molecular orbital (LUMO). Generally, the low the HOMO energy (E_{HOMO}) is, the more difficult a salt loses an electron in solvent. Frontier molecular orbital energies and corresponding experimental E_{OXs} of these existing typical eight salts in mixed solvents are shown in Table 3 [6,19,20,22-25]. The correlation between the E_{HOMO} and the corresponding E_{OX} could be generalized as a linear relationship, as showed in Fig. 8a. The correlation coefficient is 0.98. From the frontier molecular orbital energy of $LiBF_2SO_4$, the corresponding E_{OX} is estimated as 4.51 V. Not surprisingly, this numerical value of E_{OX} is very different from the one shown in Fig. 5.

In order to evaluate the E_{HOMO}-E_{OX} predictive method, some verification experiments are taken by the measurement of electrochemical windows for four typical lithium salts. The results are shown in Fig. 8b. It can be seen that the oxidation current increased first slowly then sharply. If the E_{OX} is evaluated by the initial current increase, the stability order against oxidative decomposition is: LiODFB (~4.3 V) < LiBOB (~4.4 V) < $LiBF_2SO_4$(~4.5 V) < $LiPF_6$(~4.9 V), as emphasized in Fig. 8c. The order is in good agreement with results shown in Fig. 5, and the numerical values for LiODFB, LiBOB and LiPF6 gotten by the experimental measurement are close to the data reported earlier (Table 3). So in this case, we can conclude that the credible E_{OX} for $LiBF_2SO_4$ is about 4.5 V.

Table 3. Frontier molecular orbital energies and corresponding experimental E_{OXs} of different lithium salts.

Molecule	E_{HOMO}/(kJ mol^{-1})	E_{OX} vs.(Li/Li$^+$)/V
LiBBB	-567.2130	3.6[6]
LiBOB	-777.0430	4.5[19]
LiODFB	-810.5969	4.3[20]
LiMOB	-761.1325	4.3[20]
LiFOP	-846.1199	4.5[21]
$LiBF_4$	-982.0158	5.1[22]
$LiPF_6$	-1018.3527	5.2[23]
$LiClO_4$	-814.0888	4.5[24]
$LiBF_2SO_4$	-825.2209	4.51

More than that, it is very interesting that E_{OXs} for other novel salts could be calculated by using the correlation between the E_{HOMO} and the corresponding E_{OX}, just as shown in Fig. 8a. That is, in view of the obvious inaccuracy for the predictive Eoxs shown in Fig. 5 and the inevitable errors in experiments, E_{HOMO}-E_{OX} method may a simple and accurate method to predict E_{OX}.

Reduction decomposition mechanism of $LiBF_2SO_4$.

Earlier research in the area of lithium chelato-borate and chelato-phosphate salts (such as LiBOB, LiODFB, LiFOP and $LiBF_2SO_4$) has found the general trend that many of them have a prior reduction decomposition at about 1.7 V (vs Li/Li$^+$) by the cycle voltammetry data [6,16,26]. Usually, the reduction decomposition potential is considered to correlate qualitatively closely with the energy level of the lowest unoccupied molecular orbital (LUMO). For example, the E_{LUMO} shakes around -230 kJ mol^{-1} for LiBOB (-245.274 kJ mol^{-1}), LiODFB (-222.8787 kJ mol^{-1}) and LiFOP (-261.6836 kJ mol^{-1}), respectively. However, unfortunately, this does not apply to $LiBF_2SO_4$ salt, whose E_{LUMO} is -44.607 kJ mol^{-1}. We can see that the E_{LUMO} of $LiBF_2SO_4$ is large deviation from -230 kJ mol^{-1}, though its reduction decomposition potential is about 1.7 V (vs Li/Li$^+$). To solve this confusion, the method of electronic static potential (ESP), which is commonly utilized to display the polarity and stability of molecules, is employed.

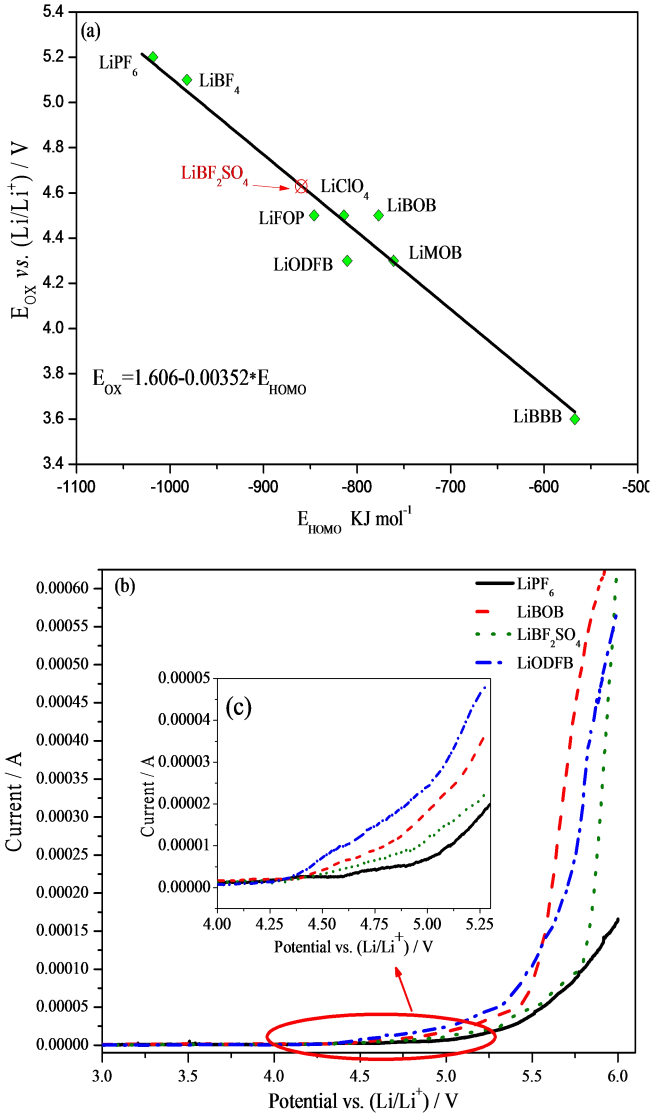

Fig. 8. (a) A linear relationship between E_{OX} and E_{HOMO} for lithium salts and (b) current potential curves of four typical salts in EC/DMC solvents.

Fig. 9 shows the ESP mapped on the isosurface (0.001 au) of electronic density of $BF_2SO_4^-$ and $ODFB^-$ radicals, respectively. The strong positive electrostatic potential exists in the boron-fluorine covalent bond (32 kcal/mol), and two negative electrostatic potential areas appear along the extension of the oxygen-sulfur and carbon-carbon covalent bonds (-44 kcal/mol). This leads to a large polarity in $BF_2SO_4^-$ and $ODFB^-$ radicals. Due to the fact that negative electrostatic potential areas are apt to collect electron, we believe that the reduction reaction will occur in different parts for different radicals. That is, the ring-opening reduction reaction will take place by breaking oxygen-sulfur covalent bond for $BF_2SO_4^-$ radical and carbon-carbon covalent bond for $ODFB^-$ radical, respectively. Maybe this is the reason why reduction decomposition potentials for $BF_2SO_4^-$ and $ODFB^-$ radicals are very close to each other, though there is a big difference in E_{LUMO}.

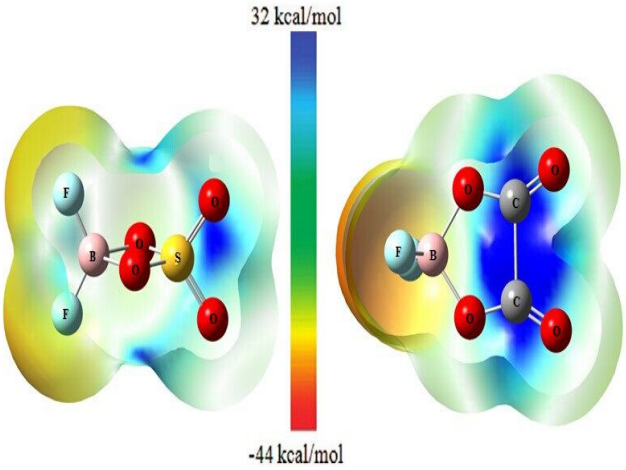

Fig. 9. Electrostatic potential for $BF_2SO_4^-$ (left) and ODFB$^-$ (right) radicals.

Both of reduction decomposition mechanism of $LiBF_2SO_4$ and possible reaction process in solvent phase have been studied. The selection of the geometric parameters is controlled by the potential energy surface of related products, and the corresponding energy is obtained by B3LYP/6-311++G(d, p) method. As shown in Fig. 10, the initial reductive decomposition of the $LiBF_2SO_4$-C involves one electron transfer from anode to a $LiBF_2SO_4$ molecule, resulting in a radical anion $[LiBF_2SO_4]^-$ (intermediate product 2). In accordance with the population analysis of spin density, unpaired electron is focused on sulfur atom. And the ring-opening reaction of the radical anion $[LiBF_2SO_4]^-$ will occur by breaking oxygen-sulfur covalent bond, due to the weakening of oxygen-sulfur bonding strength. That is in accordance with conclusions getting from Fig. 9.

The decomposition reaction of the radical anion $[LiBF_2SO_4]^-$ would proceed mainly via two paths. Path 1, $[LiBF_2SO_4]^-$ will combine with two Li^+ ions to generate SO_2 (product 3), LiF (product 4) and $LiBO_2$·LiF (product 5), via a complex transition state product of TS1. As reported, inorganic compound of SO_2 will be further reduced to form good passivation surface species, such as Li_2S and $Li_2S_2O_4$ on the graphite surface [27]. And then, the stability of SEI layer will be promoted and the impedance will be decreased [27,28]. And Path 2, $[LiBF_2SO_4]^-$ will combine with two Li^+ ions and an EC molecule to generate Li_2CO_3 (product 7), C_2H_4 (product 8) and ring-opening $LiBF_2SO_4$-A (product 9), via a complex intermediate product of 6. Then the resulting intermediate product 9 will be further decomposed to form Li_2SO_4 (product 10) and another complex transition state product of TS2. Finally, with the presence of products 4 and 5, TS2 will change into $LiBF_4$ (product 11) and $LiBO_2$ (product 12). So, we believe that a slow decomposition of $LiBF_2SO_4$ will occur during the first discharge, which is accompanied by the generation of borate radicals and rich sulfurous compounds in SEI layer. And the conductivity of the resulting SEI layer will be improved, due to the fact that rich sulfurous compounds (such as Li_2S, $Li_2S_2O_4$, and Li_2SO_4) contained in SEI layer are better conductors of Li^+ ions than analogical carbonates.

Besides, because of the energy barrier of path 1 (9.57 eV) is lower than that of path 2 (13.06 eV), we can infer that $[LiBF_2SO_4]^-$ tends to be decomposed via path 1 at the initial discharge stage in the first cycle. That is verified by the E_{LUMO} calculation. The calculation value of E_{LUMO} for 2-2Li^+ is -0.287 eV, which is significantly lower than that for 2-2Li^+-EC (-0.107 eV). So, it indicates that at high potential about 1.7 V (vs Li/Li^+), $[LiBF_2SO_4]^-$ is probably prior reduced via path 1 (2-2Li^+), rather than the co-reduction of 2-2Li^+-EC [29,30].

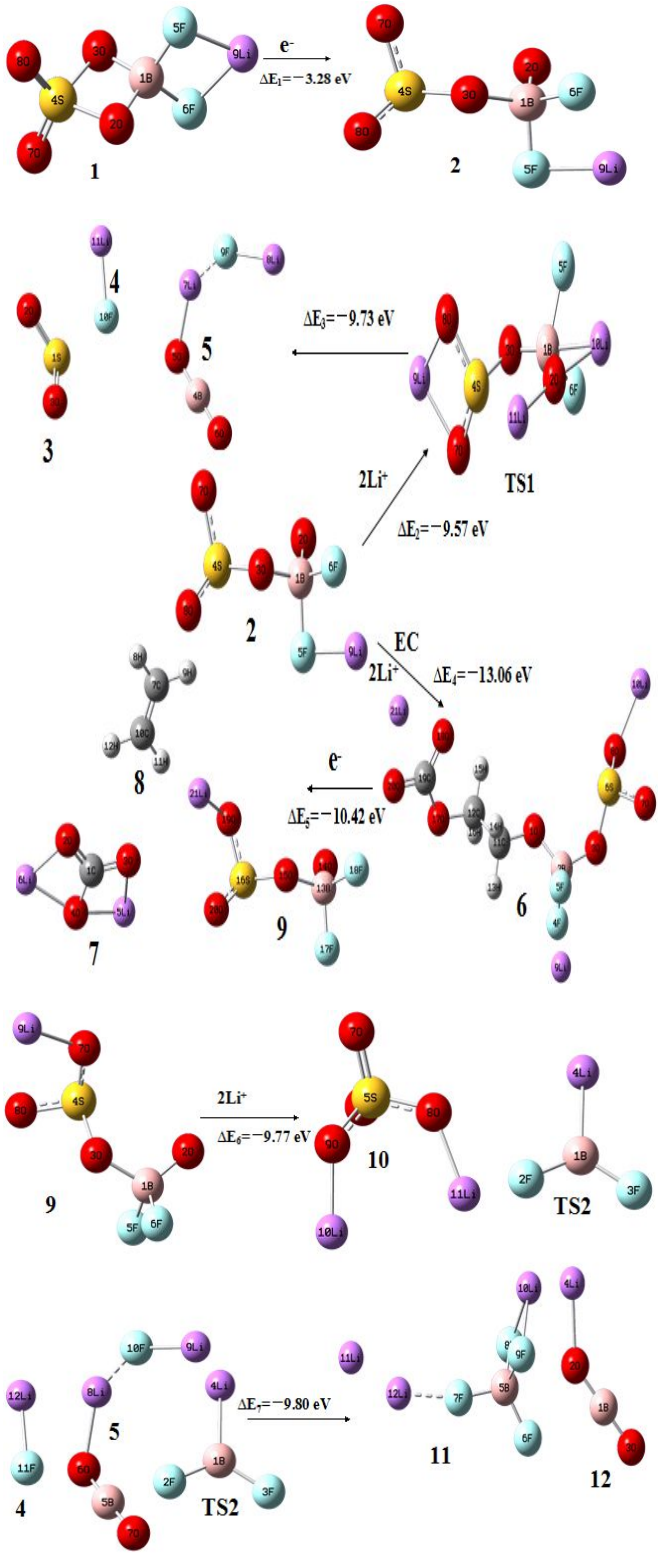

Fig. 10. Reduction decomposition mechanism of $LiBF_2SO_4$ and possible reaction process in solvent phase. The C, H atoms are represented, respectively, by gray and white spheres.

Conclusions

Both of the oxidative stability and the reduction decomposition mechanism of $LiBF_2SO_4$ have been studied by DFT calculation. The results show that oxidation potential (E_{OX}) for $LiBF_2SO_4$ could be calculated by using the correlation between the highest occupied molecular orbital energy and the corresponding E_{OX}. That is in accordance with experimental details. Besides, we infer that $LiBF_2SO_4$ itself is probably prior reduced at high potential about 1.7 V (vs Li/Li^+), due to the reduction decomposition analysis. These results is help to broaden the current knowledge of the use of chelato-borates as electrolyte components, to design and select high-performance electrolyte salts for lithium ion batteries, and to predict the chemical and physical characteristics of screening electrolyte salts, with the intent of using this induction for up-coming projected missions.

Acknowledgements

This work was supported by the Science and Technology Planning Project of Gansu Province (no. 1310RJZA043), the Natural Science Foundation of China (no. 21406100), the Science and Technology Support Project of Gansu Province (no. 144GKCB029) and the Special Fund of Gansu Province for the Transformation of Scientific and Technological Achievements for Young Talents. We acknowledge computing resources and time on the Supercomputing Center of Cold and Arid Region Environment and Engineering Research Institute of Chinese Academy of Sciences and Supercomputing Environment of Chinese Academy of Sciences.

Notes and references

[a,*] College of Petrochemical Technology, Lanzhou University of Technology, Lanzhou 730050, China. Fax: +86-931-2973648; Tel: +86-931-2973305; E-mail: xlcuilw@163.com

References

1 Armand. M.; Tarascon. J. M, Nature, 2008, 451, 652-657.
2 Ji. L. W, Lin. Z, Alcoutlabi. M, Zhang. X. W, Energy Environ. Sci, 2011, 4,2682-2699.
3 Xu. K, Chem. Rev, 2004, 104, 4303-4418.
4 Arrebola. J, Caballero. A, Hernán. L, Morales. J, Castellón. E. R, Barrado. J. R. R, J. Electrochem. Soc, 2007, 154, A178-A184.
5 Kaymaksiz. S, Wilhelm. F, Wachtler. M, Mehrens. M. W, Hartnig. C, Tschernych. I, Wietelmann. U, J. Power Sources, 2013, 239, 659-669.
6 Li. S. Y, Zhao. W, Zhao. Y. Y, Li. X. P, Cui. X. L, RSC Adv, 2013, 3, 14942-14945.
7 Han. Y. K, Jung. J, Yu. S, Lee. H, J. Power Sources, 2009, 187, 581–585.
8 Frisch. M. J, Trucks. G. W, Schlegel. H. B, Scuseria. G. E, Robb. M. A, Cheeseman. J. R, Scalmani. G, Barone. V, Mennucci. B, Petersson. G. A, et al. Gaussian 09, revision A; Gaussian, Inc.: Wallingford, CT, 2009.
9 Becke. A. D, J. Chem. Phys, 1993, 98, 5648–5652.
10 Lee. C. T, Yang. W. T, Parr. R. G, Phys. Rev. B, 1988, 37, 785–789.
11 Borodin. O, Behl. W, Jow. T. R, J. Phys. Chem. C, 2013, 117, 8661–8682.
12 Wang. R. L, Buhrmester. C, Dahn. J. R, J. Electrochem. Soc, 2006, 153, A445-A449.
13 Li. T. T, Xing. Li. D, Li. W. S, Wang. Y. T, Xu. M. Q, Gu. F. L, Hu. S. J, J. Power Sources, 2013, 244, 668–674.
14 Miertus. S, Scrocco. E, Tomasi. J, Chem. Phys, 1981, 55, 117-129.
15 Li. S. Y, Zhao. Y. Y, Shi. X. M, Li. B. C, Xu. X. L, Zhao. W, Cui. X. L, Electrochim. Acta, 2012, 65, 221-227.
16 Li. S. Y, Zhao. W, Cui. X. L, Zhao. Y. Y, Li. B. C, Zhang. H. M, Li. Y. L, Li. G. X, Ye. X. S, Luo. Y. C, Electrochim. Acta, 2013, 91, 282–292.
17 Francisco. J. S, Williams. I. H, J. Phys. Chem, 1990, 94, 8522-8529.
18 Han. S. D, Allen. J. L, Jónsson. E, Johansson. P, McOwen. D. W, Boyle. P. D, Henderson. W. A, J. Phys. Chem. C, 2013, 117, 5521–5531.
19 Sasaki. Y, Handa. M, Kurashima. K, Tonuma. T, Usami. K, J. Electrochem. Soc, 2001, 148, A999-A1003.
20 Huang. J. Y, Fan. L. Z, Yu. B. T, Xing. T. F, Qiu. W. H, Ionics, 2010,16, 509-513.
21 Ha. S. Y, Han. J. G, Song. Y. M, Chun. M. J, Han. S. I, Shin. W. C, Choi. N. S, Electrochim. Acta, 2013, 104, 170-177.
22 Zhou. L, Dalavi. S, Xu. M, Lucht. B. L, J. Power Sources, 2011, 196, 8073-8084.
23 Watanabe. Y, Kinoshita. S, Wada. S, Hoshino. K, Morimoto. H, Tobishima. S. I, J. Power Sources, 2008, 179, 770-779.
24 Hayashi. K, Nemoto. Y, Tobishima. S, Yamaki. J, Electrochim. Acta, 1999, 44, 2337-2344.
25 Aravindan. V, Gnanaraj. J, Madhavi. S, Liu. H. K, Chem. Eur. J, 2011, 17, 14326 – 14346.
26 Nagahama. M, Hasegawa. N, Okada. S, J. Electrochem. Soc, 2010, 157, A748-752.
27 Agubra. V. A, Fergus. J. W, J. Power Sources, 2014, 240, 153–162.
28 Cui. X. L, Zhang. H. M, Li. S. Y, Zhao. Y. Y, Mao. L. P, Zhao. W, Li. Y. L, Ye. X. S, J. Power Sources, 2013, 240, 476–485.
29 Xing. L. D, Li. W. S, Wang. C. Y, Gu. F. L, Xu. M. Q, Tan. C. L, Y. J, J. Phys. Chem. B, 2009, 113, 16596-16602.
30 Leggesse. E. G, Jiang. J, J. Phys. Chem. A, 2012, 116, 11025-11033.